Earth Syst. Dynam. Discuss., 5, 991–1012, 2014
www.earth-syst-dynam-discuss.net/5/991/2014/
doi:10.5194/esdd-5-991-2014

Earth System Dynamics Discussions
Open Access

Differences in carbon cycle and temperature projections from emission- and concentration-driven earth system model simulations

P. Shao[1], X. Zeng[1], and X. Zeng[2]

[1]International Center for Climate and Environment Sciences, Institute of Atmospheric Physics, Chinese Academy of Sciences, Beijing, China
[2]Department of Atmospheric Sciences, University of Arizona, Tucson, AZ, USA

Received: 8 August 2014 – Accepted: 21 August 2014 – Published: 29 August 2014

Correspondence to: P. Shao (shaopu0608@gmail.com)

Published by Copernicus Publications on behalf of the European Geosciences Union.

Abstract

The influence of prognostic and prescribed atmospheric CO_2 concentrations ($[CO_2]$) on the carbon uptake and temperature is investigated using all eight Earth System Models (ESMs) with relevant output variables from the Coupled Model Intercomparison Project Phase 5 (CMIP5). Under the RCP8.5 scenario, the projected $[CO_2]$ differences in 2100 vary from −19.7 to +207.3 ppm in emission-driven ESMs. Incorporation of the interactive concentrations also increases the range of global warming, computed as the 20 year average difference between 2081–2100 and 1850–1869/1861–1880, by 49 % from 2.36 K (i.e. ranging from 3.11 to 5.47 K) in the concentration-driven simulations to 3.51 K in the emission-driven simulations. The observed seasonal amplitude of global $[CO_2]$ from 1980–2011 is about 1.2–5.3 times as large as those from the eight emission-driven ESMs, while the $[CO_2]$ seasonality is simply neglected in concentration-driven ESMs, suggesting the urgent need of ESM improvements in this area. The temperature-concentration feedback parameter α is more sensitive to $[CO_2]$ (e.g. during 1980–2005 versus 2075–2100) than how $[CO_2]$ is handled (i.e. prognostic versus prescribed). This sensitivity can be substantially reduced by using a more appropriate parameter α' computed from the linear regression of temperature change versus that of the logarithm of $[CO_2]$. However, the inter-model relative variations of both α and α' remain large, suggesting the need of more detailed studies to understand and hopefully reduce these discrepancies.

1 Introduction

Human activities emit carbon dioxide (CO_2) into the earth system, and this emission can be partitioned into the change of carbon in the atmosphere, land, and ocean. This partitioning can be simulated using Integrated Assessment Models (IAMs) (Van Vuuren et al., 2011a) or sophisticated earth system models (ESMs). Compared with ESMs, IAMs include substantially simplified treatments of dynamic, physical, chemical, and

ESDD
5, 991–1012, 2014

biological processes in the earth system, but they do treat human activities including the land use change in more detail (Van Vuuren et al., 2011b). Some of the treatments from IAMs, in turn, have also been adopted by ESMs, such as the dynamic land-use distributions in the Geophysical Fluid Dynamics Laboratory (GFDL)'s and Met Office Hadley Centre's ESM families (Shevliakova et al., 2009; Jones et al., 2011).

For earlier (1st to 4th) Assessment Reports of the Intergovernmental Panel on Climate Change (IPCC), IAMs were used to provide the atmospheric carbon concentration ($[CO_2]$) trajectories that were then used by climate models to assess the physical science basis of climate change. For the current 5th Assessment Report (AR5) of IPCC, most of the ESMs include the interactive carbon cycle in the atmosphere, land, and ocean biogeochemical components, and hence can be run using prescribed $[CO_2]$ (referred to as "concentration-driven") from IAMs like before or using prescribed anthropogenic emissions (referred to as "emission-driven"). In the emission-driven experiment, the variation of $[CO_2]$, as the residual of emissions minus the land and ocean carbon uptakes, is caused by internal and external forcings and their complex interactions through the explicit carbon processes within the ESMs. The diagnosed cumulative emissions are mostly contributed by the carbon-concentration feedback that is about 4.5 times larger than the carbon-climate feedback (Arora et al., 2013). In contrast, the concentration-driven experiments include one-way coupling only: while the $[CO_2]$ trajectories affect other (e.g. physical, chemical, and biological) processes, they are not affected by these processes in ESMs.

There are inevitable differences in the carbon uptake and climate between the concentration- and emission-driven simulations because of the model-dependent climate-carbon cycle feedbacks. Jones et al. (2013) showed that the fossil fuel emissions modeled by the ESMs participating in the Coupled Model Intercomparison Project (CMIP5) agree well with reconstructions over the historical period, and they are consistent with the IAMs for the Representative Concentration Pathways (RCPs) RCP2.6 and RCP4.5 but smaller compared to RCP6.0 and RCP8.5 in the future projections. Booth et al. (2013) argued that the emission-driven ESMs broaden ranges of projected

ESDD
5, 991–1012, 2014

temperature responses compared to the concentration-driven simulations, especially for the models exhibiting climate sensitivities above 4.5 K. However, their conclusion was not based on the direct comparison of emission- and concentration-driven simulations for each ESM. Friedlingstein et al. (2014) found that seven out of eleven ESMs under RCP8.5 simulate a larger [CO_2] and hence higher radiative forcing (on average by 44 ppm and by 0.25 W m^{-2}, respectively) in the emission-driven simulations by 2100, leading to higher temperature projections than in the concentration-driven simulations. However, they omitted the analysis of historical simulations. Previous studies have also demonstrated that the uncertainty in [CO_2] projections is mainly attributable to uncertainties in the response of the land carbon cycle (Jones et al., 2013; Friedlingstein et al., 2014), and the higher ends of climate projections are significantly warmer in the emission-driven simulations because of stronger carbon cycle feedbacks (Arora et al., 2013; Friedlingstein et al., 2014).

The seasonal cycle of [CO_2] is neglected in concentration-driven ESMs but it is considered in emission-driven simulations. There is a model consensus among the CMIP5 ESMs that the seasonal amplitude of [CO_2] continues to increase throughout the 21st century mostly due to enhanced ecosystem uptake during the Northern Hemisphere growing season (Zhao and Zeng, 2014), but its trend for the historical period is not well simulated (Graven et al., 2013). The use of the observed seasonal cycle of [CO_2] to constrain the parameterization of terrestrial processes in ESMs was also emphasized in Alexandrov (2014).

To help quantify the feedbacks between carbon cycle and climate, Friedlingstein et al. (2006) proposed the carbon-concentration and carbon-climate feedback parameters, which were further discussed and developed by Arora et al. (2013) and Boer and Arora (2013). While the temperature-[CO_2] feedback can be directly computed from emission- and concentration-driven CMIP5 simulations, the separation of the carbon–climate and carbon–concentration feedbacks requires additional simulations (e.g. the simulation with 1 % increase of [CO_2] per year; see Arora et al., 2013).

ESDD
5, 991–1012, 2014

Building upon these studies, the purpose of this study is to quantify and understand the differences in carbon cycle and temperature projections from emission- and concentration-driven CMIP5 simulations. Specifically two questions will be addressed: how large are the differences in the carbon uptake, [CO_2], and temperature from these two types of experiments, and how can we characterize the temporal variation of temperature-[CO_2] feedback in each ESM between these experiments? The eight ESMs and the emission- and concentration-driven simulations are discussed in Sect. 2, while the results are presented in Sect. 3. The conclusions are given in Sect. 4.

2 Models and simulations

We choose ESMs with relevant output variables from at least one ensemble member for the historical (1850–2005 or 1861–2005) and future (2006–2100) simulations. Among the four future RCPs (RCP2.6, RCP4.5, RCP6.0, and RCP8.5) (Moss et al., 2010) developed for CMIP5 which has been set up as a major input into AR5, RCP8.5 is the only emission-driven core experiment proposed for CMIP5 exercise. Therefore, here we choose the high-emission RCP8.5 scenario under which the total radiative forcing estimated by the IAMs will be around 8.5 $W\,m^{-2}$ in 2100. The differences between the concentration- and emission-driven simulations are expected to be smaller in magnitude for other scenarios if they are implemented (Booth et al., 2013). In this way, only eight ESMs from the CMIP5 are available and selected: BUN-ESM, CanESM2, CESM1-BGC, GFDL-ESM2G, GFDL-ESM2M, INMCM4, MIROC-ESM, and MPI-ESM-LR. Four of them (BNU-ESM, CESM1-BGC, MIROC-ESM, and MPI-ESM-LR) produced time-varying three-dimensional [CO_2] in the emission-driven experiments which need to be vertically and horizontally integrated to provide globally averaged [CO_2] used in our analysis. Taylor et al. (2012) discussed in detail the setup of the CMIP5 experiments, and Arora et al. (2013) gave an initial analysis of the CMIP5 emission-driven runs with a brief introduction to some of the ESMs used here.

ESDD
5, 991–1012, 2014

The preset value of $[CO_2]$ in the concentration-driven simulations is harmonized to be consistent with the observations and inventories by the MAGICC model (Meinshausen et al., 2011) for the historical period and developed by an IAM (i.e. MESSAGE) (Van Vuuren et al., 2011b) for the RCP8.5 scenario. These global annual mean values are linearly interpolated to each month for use in the ESMs. The corresponding CO_2 emissions from fossil fuel simulated by these IAMs are used in emission-driven ESM simulations. The emissions of other greenhouse gases and aerosols are treated as externally specified in both types of simulations. The RCP8.5 repository also includes the land use change (LUC) emission data, but the use of these data differs among ESMs.

3 Results

3.1 Differences in the carbon uptake, $[CO_2]$, and temperature from emission- and concentration-driven simulations

The annual differences in the atmospheric CO_2 mass between emission- and concentration-driven simulations show very different temporal variations across the ESMs from 1850 to 2100 (Fig. 1a). GFDL-ESM2G and GFDL-ESM2M have the positive differences for the whole period. The differences in MPI-ESM-LR show alternatively positive and negative variations on a time-scale of several tens of years and stay positive over the last three decades. The results of BNU-ESM, CanESM2, CESM1-BGC, and MIROC-ESM show negative differences followed by positive values. INMCM4 has positive differences between 2001 and 2066 but negative values before or after this period. Given the approximate conversion factor of 1 ppm $[CO_2]$ increase per 7.77 Pg CO_2 that remains in the atmosphere, the $[CO_2]$ differences vary from −3.0 ppm in MPI-ESM-LR to 18.3 ppm in CESM1-BGC by 2005 (Table 1). These differences become much larger in magnitude by 2100: from −19.7 ppm (in INMCM4) to +207.3 ppm (in MIROC-ESM), or from −2.1 to +22.1 % compared with $[CO_2]$ in 2100

ESDD
5, 991–1012, 2014

in the concentration-driven simulations (Table 1). The highest bias in MIROC-ESM by 2100 is probably due to its strong land carbon-climate feedback (Arora et al., 2013).

These [CO_2] differences are related to the land and ocean accumulated carbon uptake differences between emission- and concentration-driven simulations (Fig. 1b and c). The changes in land and ocean carbon pools range from about −184.3 to +245.0 Pg CO_2 by 2100. Here an outlier of large terrestrial assimilation reduction in INMCM4 is excluded, largely because INMCM4 uses prescribed LUC emissions as an external forcing rather than calculates the emissions from the imposed land cover change scenarios. The accumulated differences by 2100 over land are close to or slightly greater than those over ocean in all ESMs (Fig. 3b and c), since terrestrial differences show more spatial heterogeneities and have larger magnitudes in individual grid boxes (not shown). The concentration-driven carbon uptake in CanESM2 is weaker over ocean and stronger over land than the observations for the 1850–2005 period (Arora et al., 2011), and this bias becomes worse in the emission-driven simulation as indicated by the negative differences over ocean (Fig. 1c) and positive differences over land (Fig. 1b) by 2005. Generally, the oceanic solubility pump and organic and carbonate pumps are relatively simple and spatially homogenous compared to the terrestrial carbon uptake, so the oceanic difference curves are much smoother from year to year. Since positive carbon uptakes over land and ocean are associated with negative changes of [CO_2], the contributions from all ESMs except INMCM4 to the change in [CO_2] by 2100 vary from −20.7 to +23.7 ppm over land, and vary from −31.5 to −0.9 ppm over ocean. The abnormal terrestrial contribution in INMCM4 is as large as +139.4 ppm with a much smaller oceanic contribution of −1.5 ppm.

Note that the comparable accumulated differences (between emission- and concentration-driven simulations) by 2100 over land versus over ocean in Fig. 1b and c do not contradict with previous studies based on emission-driven simulations only. For instance, the inter-model discrepancy on a global scale was found to be dominated by the diverse treatments of the land carbon cycle as the processes that determine ocean carbon uptake are generally similar across the models (Arora et al., 2013; Friedlingstein

ESDD
5, 991–1012, 2014

et al., 2014). The general positive [CO_2] differences by the end of historical period are partly contributed by the weak ocean carbon uptake (Hoffman et al., 2014). Also following Hoffman et al. (2014), we have computed the ratio of ocean carbon accumulation over atmospheric accumulation in the emission-driven simulation for each ESM. The median of modelled ratios declines from 0.60 by 2005 to 0.29 by 2100. This indicates the relative weakening of ocean carbon uptake, contributing to the larger [CO_2] differences between emission- and concentration-driven simulations in the 21st century (Fig. 1a).

Based on mass conservation in the earth system, the total anthropogenic carbon emission can be computed as the sum of changes in the three carbon pools (atmosphere, land, and ocean). The same approach was used in Jones et al. (2013) and Gillett et al. (2013). Hoffman et al. (2014) used a slightly different approach by including carbon fluxes due to LUC implicitly in the land carbon pool. Figure 1d shows that the differences of diagnosed emissions between emission- and concentration-driven simulations differ substantially among ESMs. By 2100, these differences vary from −1225 Pg CO_2 in INMCM4 to +1854 Pg CO_2 in CESM1-BGC (or −17.6 and +21.5 % of the total emissions from the corresponding emission-driven simulations of these models). These differences are caused by the differences in carbon gains because of CO_2 fertilization and carbon loss from LUC and warming. The negative difference in INMCM4 is mostly owing to its failure to properly represent carbon release to the atmosphere associated with land-use change, while the large positive differences in CanESM2 and CESM1-BGC are due to their higher climate-carbon cycle feedback than the IAMs (Jones et al., 2013; Piao et al., 2013).

Besides the annual mean [CO_2] differences between emission- and concentration-driven simulations, seasonal [CO_2] differences are also expected for obvious reasons (Fig. 2a). The seasonal cycle of [CO_2] in emission-driven simulations is primarily driven by the vegetation photosynthesis and respiration seasonality over land, and the observed [CO_2] (GLOBALVIEW-CO2, 2012) reaches its maximum in April–May and minimum in August–September. Among the eight ESMs, MPI-ESM-LR shows the

ESDD
5, 991–1012, 2014

best performance, but its seasonal amplitude (3.55 ppm) is still just 83 % of the observed value (4.29 ppm) followed by MIRCO-ESM (2.70 ppm) and the two GFDL models (around 2.2 ppm). The other four ESMs have much weaker seasonal amplitudes. They also have phase errors; e.g., the minimum value occurs in October in CanESM2 and CESM1-BGC and in July in INMCM4.

All the ESMs have minimal [CO_2] seasonality in concentration-driven simulations, because they linearly interpolate the prescribed annual mean [CO_2] to the atmospheric carbon pool uniformly. Note that CESM1-BGC (and BNU-ESM whose atmospheric component is based on CESM1-BGC) also computes a three-dimensional CO_2 tracer driven by land and ocean surface CO_2 fluxes as well as fossil fuel emissions in the concentration-driven simulations. The resulting global average [CO_2] does have a seasonal cycle, and this seasonality is nearly the same as that in the emission-driven simulation. However, the CO_2 tracer is purely diagnostic and its values are not used by any radiative or biogeochemical computation (K. Lindsay, personal communication, 2013) and hence are not discussed here.

The global annual mean temperature is also different between the emission- and concentration-driven simulations due to the radiative and biogeochemical effects of [CO_2] (Fig. 3a), and the differences vary from −0.36 K (in INMCM4) to +1.10 K (in MIROC-ESM) in the year 2100. These differences are larger over land (from −0.51 to +1.58 K) (Fig. 3b) than over ocean (from −0.29 to +0.92 K) (Fig. 3c). The global warming spreads from 3.11 to 5.47 K (computed as the 20 year average difference between 2081–2100 and 1850–1869/1861–1880) in concentration-driven simulations across different ESMs (Table 1). The corresponding additional warming/cooling with a range of −0.21 to +0.94 K in emission-driven simulations (Table 1) are −6.8 to +17.2 % of the above warming from 1850/1861 to 2100. In particular, the spread in the warming among the eight ESMs increases from 2.36 K (= 5.47 – 3.11) in concentration-driven simulations to 3.51 K (= 6.50 – 2.99) in emission-driven simulations.

The correlation coefficients between the simulated and observed global annual mean temperature from HadCRUT4.2 (Morice et al., 2012) over 1850–2005/1861–2005

ESDD
5, 991–1012, 2014

are all positive and significant at the 0.01 level. They change little between the concentration- and emission-driven simulations (Table 1), suggesting that there is no significant change in the hindcast skill of long-term temperature trends during this period.

3.2 The temperature-[CO_2] feedback

There are various metrics of climate-carbon cycle feedbacks useful for the model intercomparison and climate change mitigation policy (Friedlingstein et al., 2006; Gillett et al., 2013). There is no reason to expect a linear model to accurately characterize the nonlinear climate system, as the system is sensitive to the temporal rate of change in [CO_2] trajectory as well as its mean state. Nevertheless the feedback parameters provide insight into the behavior of the coupled carbon-climate system and also provide a useful common framework for comparing models (Arora et al., 2013). For instance, the change of [CO_2] is closely associated with the change of temperature and then the climate sensitivity parameter α can be obtained through a linear regression:

$$\Delta T = \alpha \Delta [CO_2] + b \quad (1)$$

where ΔT and $\Delta[CO_2]$ are the changes of global annual mean temperature and [CO_2] relative to the beginning of the historical simulations, with b representing the intercept. When Eq. (1) is applied to the differences between two simulations (e.g. between simulations with constant [CO_2] with time versus doubling of [CO_2]), $b = 0$, and α becomes the same as that defined in Friedlingstein et al. (2006). The smallest α in INMCM4 among the eight ESMs in Table 2 is consistent with the finding in Booth et al. (2013) that temperature is least sensitive to the same magnitude of variation in [CO_2] in INMCM4 compared to other CMIP5 ESMs. The multi-model mean α values during the period of 1980–2005 are nearly the same (1.45 versus 1.44 K per 100 ppm) between the concentration- and emission-driven simulations, and they are 17–18 % higher than the observation-based estimation (1.23 K per 100 ppm). However, the upper and lower

ESDD
5, 991–1012, 2014

bounds of α are changed in different experiments, leading to a narrower range in the emission-driven simulations (Table 2).

Table 2 shows that α decreases significantly from the period of 1980–2005 to 2075–2100 in all ESMs. Since the radiative forcing and hence temperature change is more likely associated with the logarithm of $[CO_2]$ rather than $[CO_2]$ itself (Cadule et al., 2009), we can define a similar feedback coefficient α' from:

$$\Delta T = \alpha' \Delta \ln[CO_2] + b. \quad (2)$$

Table 2 shows that indeed, the relative variation of α' from the period of 1980–2005 to 2075–2100 is overall much smaller than that of α. For instance, the median of α decreases by a factor of 2.72 from 1.42 to 0.52 K per 100 ppm in the concentration-driven simulations from 1980–2005 to 2075–2100, while the median of α' decreases by 15 % only from 5.08 to 4.32 K. Based on Eqs. (1) and (2), α equals α' divided by $[CO_2]$. Therefore, the large decrease of α from 1980–2005 to 2075–2100 can be partially explained by the increase of $[CO_2]$ by a factor of ~2.3. On the other hand, the inter-model discrepancy remains large; for instance, the standard deviation of α relative to its mean is 0.376 in the concentration-driven experiments, very close to that of α' (0.375) in the emission-driven experiments over 1980–2005.

A similar comparison was done over a longer period of 51 years (from 1955–2005 and from 2050–2100) with similar conclusions. For instance, the multi-model median of α decreases by a factor of 2.27 in the concentration-driven simulations from 1955–2005 to 2050–2100, while the median of α' decreases by 6.9 % only. Therefore, α' is less sensitive than α to the period used for calculation, and hence represents a more robust metric to quantify the temperature-$[CO_2]$ feedback in different periods.

The values of α' are helpful to understand the differences between the emission- and concentration-driven simulations discussed in Sect. 3.1. For instance, the $[CO_2]$ difference by 2100 is similar for CESM1-BGC and MIROC-ESM (Fig. 1a), and it is much greater than that by 2000. Therefore, this $[CO_2]$ difference by 2100 can be approximated by the difference of $[CO_2]$ difference (at 2100 versus at 2000) between the

ESDD
5, 991–1012, 2014

emission- and concentration-driven simulations. Because of the larger α' values in the 21st century from MIROC-ESM (Table 2), the temperature difference by 2100 is much larger in MIROC-ESM than in CESM1-BGC (Fig. 3a).

The monthly temperature-[CO_2] relationship within a year is very different from that the annual relationship discussed so far. With the small [CO_2] seasonality, the temperature seasonality is nearly the same between the two types of simulations (Fig. 2b and c). Furthermore, the annual cycles of temperature in all ESMs (except CanESM2 over Northern Hemisphere and BNU-ESM over both hemispheres) agree well with observations.

4 Conclusions

The differences of [CO_2], land and ocean carbon uptakes, and surface air temperature between the emission- and concentration-driven simulations are investigated using all eight process-based ESMs with relevant output variables available under the CMIP5 framework. Under the RCP8.5 scenario, the [CO_2] differences by 2100 vary from −19.7 ppm in INMCM4 to +207.3 ppm in MIROC-ESM, or −2.1 to +22.1 % compared with [CO_2] in 2100 in the corresponding concentration-driven simulations. The diagnosed accumulated CO_2 emission differences in 2100 are also large, varying from −1225 Pg CO_2 in INMCM4 to +1854 Pg CO_2 in CESM1-BGC. Emission-driven simulations also significantly increase the spread in the global warming (or temperature difference between 2081–2100 and 1850–1869 or 1861–1880) across the eight ESMs by 49 % from 2.36 K (i.e. between 3.11 and 5.47 K) in the concentration-driven simulations to 3.51 K (between 2.99 and 6.50 K).

The two types of simulations even affect the relationship between the changes of temperature and [CO_2], as quantified by the climate sensitivity parameter α in Eq. (1) in each ESM, but these simulations do not affect much the ESM-averaged α. Furthermore, while α is strongly dependent on the period (with different global mean [CO_2] and temperature), this dependence is much less for α' computed from Eq. (2). Therefore,

ESDD
5, 991–1012, 2014

we suggest that α' rather than α should be used as the metric to quantify the climate-carbon cycle sensitivity. Similarly, the logarithm of $[CO_2]$ rather than $[CO_2]$ itself is suggested to be used in the computation of the feedback parameter γ (Friedlingstein et al., 2006; Boer and Arora, 2013) or the similar parameter in Gillett et al. (2013). On the other hand, the inter-model relative variations of both α and α' remain large, suggesting the need of more detailed studies (e.g. comparing α' at regional scales) to understand and hopefully reduce these discrepancies.

The observed seasonal amplitude of global $[CO_2]$ is 1.2 times the value of MPI-ESM-LR and 5.3 times the value of CanESM2, with other models falling in the range of 1.6–4.4 times. Recognizing the difficulty in validating the carbon cycle from ESMs (e.g. Shao et al., 2013), well-observed seasonal cycle of global $[CO_2]$ provides a reliable benchmark for the evaluation of emission-driven simulations. Therefore a low-hanging fruit would be to improve the seasonal cycle (including both amplitude and phase) of ESMs in emission-driven simulations.

Recognizing the differences in the carbon cycle, temperature, and their relationship in these two types of simulations, where do we go from here? Concentration-driven simulations are more strongly constrained, and they are the only simulations possible for ESMs without the full carbon cycle over land and ocean. Emission-driven simulations involve the full effects of carbon cycle feedbacks in the earth system. They are more physically consistent but are less strongly constrained. To move forward as a community, IAMs and ESMs need to be better integrated so that $[CO_2]$ from the emission-driven simulations becomes more consistent with that from IAMs and the diagnosed accumulated anthropogenic emissions from two types of simulations become more consistent. This could be facilitated by the better integration of IPCC Working Groups I and II. For instance, IAMs could consider using ESMs of intermediate complexity (Zickfeld et al., 2013) or their simplified versions under the constraint of maintaining computational efficiency, while ESMs could consider adopting the LUC treatment from IAMs.

ESDD
5, 991–1012, 2014

Acknowledgement. The first two authors were supported by NSFC (41305096) and CAS (XDA05110103), while the last author was supported by NSF (AGS-0944101) and DOE (DE-SC0006693). The authors thank the modeling groups that provide the eight ESM outputs; and the WCRP Working Group on Coupled Modeling (WGCM) for making the model output available on the Earth System Grid Federation servers (particularly at the US Department of Energy PCMDI and ORNL).

References

Alexandrov, G. A.: Explaining the seasonal cycle of the globally averaged CO_2 with a carbon cycle model, Earth Syst. Dynam. Discuss., 5, 63–81, doi:10.5194/esdd-5-63-2014, 2014.

Arora, V. K., Scinocca, J. F., Boer, G. J., Christian, J. R., Denman, K. L., Flato, G. M., Kharin, V. V., Lee, W. G., and Merryfield, W. J.: Carbon emission limits required to satisfy future representative concentration pathways of greenhouse gases, Geophys. Res. Lett., 38, L05805, doi:10.1029/2010GL046270, 2011.

Arora, V. K., Boer, G. J., Friedlingstein, P., Eby, M., Jones, C. D., Christian, J. R., Bonan, G., Bopp, L., Brovkin, V., Cadule, P., Hajima, T., Ilyina, T., Lindsay, K., Tjiputra, J. F., and Wu, T.: Carbon-concentration and carbon-climate feedbacks in CMIP5 Earth system models, J. Climate, 26, 5289–5314, doi:10.1175/JCLI-D-12-00494.1, 2013.

Boer, G. J. and Arora, V. K.: Feedbacks in emission-driven and concentration-driven global carbon budgets, J. Climate, 26, 3326–3341, doi:10.1175/JCLI-D-12-00365.1, 2013.

Booth, B. B. B., Bernie, D., McNeall, D., Hawkins, E., Caesar, J., Boulton, C., Friedlingstein, P., and Sexton, D. M. H.: Scenario and modelling uncertainty in global mean temperature change derived from emission-driven global climate models, Earth Syst. Dynam., 4, 95–108, doi:10.5194/esd-4-95-2013, 2013.

Cadule, P., Bopp, L., and Friedlingstein, P.: A revised estimate of the processes contributing to global warming due to climate-carbon feedback, Geophys. Res. Lett., 36, L14705, doi:10.1029/2009GL038681, 2009.

Friedlingstein, P., Cox, P., Betts, R., Bopp, L., Von, W., Von Bloh, W., Brovkin, V., Cadule, P., Doney, S., Eby, M., Fung, I., Bala, G., John, J., Jones, C., Joos, F., Kato, T., Kawamiya, M., Knorr, W., Lindsay, K., Matthews, H. D., Raddatz, T., Rayner, P., Reick, C., Roeckner, E., Schnitzler, K. G., Schnur, R., Strassmann, K., Weaver, A. J., Yoshikawa, C., and Zeng, N.:

ESDD

5, 991–1012, 2014

Climate-carbon cycle feedback analysis: results from the C^{4}MIP model intercomparison, J. Climate, 19, 3337–3353, doi:10.1175/JCLI3800.1, 2006.
Friedlingstein, P., Meinshausen, M., Arora, V. K., Jones, C. D., Anav, A., Liddicoat, S. K., and Knutti, R.: Uncertainties in CMIP5 climate projections due to carbon cycle feedbacks, J. Climate, 27, 511–526, doi:10.1175/JCLI-D-12-00579.1, 2014.
Gillett, N. P., Arora, V. K., Matthews, D., and Allen, M. R.: Constraining the ratio of global warming to cumulative CO_2 emissions using CMIP5 simulations, J. Climate, 26, 6844–6858, doi:10.1175/JCLI-D-12-00476.1, 2013.
GLOBALVIEW-CO2: Cooperative Atmospheric Data Integration Project – Carbon Dioxide, http://www.esrl.noaa.gov/gmd/ccgg/globalview/, NOAA ESRL, Boulder, Colorado, 2012.
Graven, H. D., Keeling, R. F., Piper, S. C., Patra, P. K., Stephens, B. B., Wofsy, S. C., Welp, L. R., Sweeney, C., Tans, P. P., Kelley, J. J., Daube, B. C., Kort, E. A., Santoni, G. W., and Bent, J. D.: Enhanced seasonal exchange of CO_2 by northern ecosystems since 1960, Science, 341, 1085–1089, doi:10.1126/science.1239207, 2013.
Hoffman, F. M., Randerson, J. T., Arora, V. K., Bao, Q., Cadule, P., Ji, D., Jones, C. D., Kawamiya, M., Khatiwala, S., Lindsay, K., Obata, A., Shevliakova, E., Six, K. D., Tjiputra, J. F., Volodin, E. M., and Wu, T.: Causes and implications of persistent atmospheric carbon dioxide biases in Earth System Models, J. Geophys. Res.-Biogeo., 119, 141–162, doi:10.1002/2013JG002381, 2014.
Jones, C. D., Hughes, J. K., Bellouin, N., Hardiman, S. C., Jones, G. S., Knight, J., Liddicoat, S., O'Connor, F. M., Andres, R. J., Bell, C., Boo, K. O., Bozzo, A., Butchart, N., Cadule, P., Corbin, K. D., Doutriaux-Boucher, M., Friedlingstein, P., Gornall, J., Gray, L., Halloran, P. R., Hurtt, G., Ingram, W. J., Lamarque, J. F., Law, R. M., Meinshausen, M., Osprey, S., Palin, E. J., Chini, L. P., Raddatz, T., Sanderson, M. G., Sellar, A. A., Schurer, A., Valdes, P., Wood, N., Woodward, S., Yoshioka, M., and Zerroukat, M.: The HadGEM2-ES implementation of CMIP5 centennial simulations, Geosci. Model. Dev., 4, 543–570, doi:10.5194/gmd-4-543-2011, 2011.
Jones, C. D., Robertson, E., Arora, V., Friedlingstein, P., Shevliakova, E., Bopp, L., Brovkin, V., Hajima, T., Kato, E., Kawamiya, M., Liddicoat, S., Lindsay, K., Reick, C. H., Roelandt, C., Segschneider, J., and Tjiputra, J.: Twenty-First-Century compatible CO_2 emissions and airborne fraction simulated by CMIP5 Earth System Models under four representative concentration pathways, J. Climate, 26, 4398–4413, doi:10.1175/JCLI-D-12-00554.1, 2013.

ESDD
5, 991–1012, 2014

Meinshausen, M., Raper, S. C. B., and Wigley, T. M. L.: Emulating coupled atmosphere-ocean and carbon cycle models with a simpler model, MAGICC6 – Part 1: Model description and calibration, Atmos. Chem. Phys., 11, 1417–1456, doi:10.5194/acp-11-1417-2011, 2011.

Morice, C. P., Kennedy, J. J., Rayner, N. A., and Jones, P. D.: Quantifying uncertainties in global and regional temperature change using an ensemble of observational estimates: the HadCRUT4 dataset, J. Geophys. Res., 117, D08101, doi:10.1029/2011JD017187, 2012.

Moss, R. H., Edmonds, J. A., Hibbard, K. A., Manning, M. R., Rose, S. K., Van Vuuren, D. P., Carter, T. R., Emori, S., Kainuma, M., and Kram, T.: The next generation of scenarios for climate change research and assessment, Nature, 463, 747–756, doi:10.1038/nature08823, 2010.

Piao, S., Sitch, S., Ciais, P., Friedlingstein, P., Peylin, P., Wang, X., Ahlström, A., Anav, A., Canadell, J. G., Cong, N., Huntingford, C., Jung, M., Levis, S., Levy, P. E., Li, J., Lin, X., Lomas, M. R., Lu, M., Luo, Y., Ma, Y., Myneni, R. B., Poulter, B., Sun, Z., Wang, T., Viovy, N., Zaehle, S., and Zeng, N.: Evaluation of terrestrial carbon cycle models for their sensitivity to climate changes and rising atmospheric CO_2 concentrations, Global Change Biol., 19, 2117–2132, doi:10.1111/gcb.12187, 2013.

Shao, P., Zeng, X.-B., Sakaguchi, K., Monson, R. K., and Zeng, X.-D.: Terrestrial carbon cycle – climate relations in eight CMIP5 earth system models, J. Climate, 26, 8744–8764, doi:10.1175/JCLI-D-12-00831.1, 2013.

Shevliakova, E., Pacala, S. W., Malyshev, S., Hurtt, G. C., Milly, P. C. D., Caspersen, J. P., Sentman, L. T., Fisk, J. P., Wirth, C., and Crevoisier, C.: Carbon cycling under 300 years of land use change: importance of the secondary vegetation sink, Global Biogeochem. Cy., 23, GB2022, doi:10.1029/2007GB003176, 2009.

Van Vuuren, D. P., Lowe, J., Stehfest, E., Gohar, L., Hof, A. F., Hope, C., Warren, R., Meinshausen, M., and Plattner, G. K.: How well do integrated assessment models simulate climate change?, Climatic Change, 104, 255–285, doi:10.1007/s10584-009-9764-2, 2011a.

Van Vuuren, D. P., Edmonds, J., Kainuma, M., Riahi, K., Thomson, A., Hibbard, K., Hurtt, G. C., Kram, T., Krey, V., Lamarque, J.-F., Masui, T., Meinshausen, M., Nakicenovic, N., Smith, S. J., and Rose, S. K.: The representative concentration pathways: an overview, Climatic Change, 109, 5–31, doi:10.1007/s10584-011-0148-z, 2011b.

Zhao, F. and Zeng, N.: Continued increase in atmospheric CO_2 seasonal amplitude in the 21st century projected by the CMIP5 Earth System Models, Earth Syst. Dynam. Discuss., 5, 779–807, doi:10.5194/esdd-5-779-2014, 2014.

ESDD
5, 991–1012, 2014

Zickfeld, K., Eby, M., Alexander, K., Weaver, A. J., Crespin, E., Fichefet, T., Goosse, H., Philippon-Berthier, G., Edwards, N. R., Holden, P. B., Eliseev, A. V., Mokhov, I. I., Feulner, G., Kienert, H., Perrette, M., Schneider von Deimling, T., Forest, C. E., Friedlingstein, P., Joos, F., Spahni, R., Steinacher, M., Kawamiya, M., Tachiiri, K., Kicklighter, D., Monier, E., Schlosser, A., Sokolov, A., Matsumoto, K., Tokos, K. S., Olsen, S. M., Pedersen, J. O. P., Ridgwell, A., Shaffer, G., Yoshimori, M., Zeng, N., and Zhao, F.: Long-term climate change commitment and reversibility: an EMIC intercomparison, J. Climate, 26, 5782–5809, doi:10.1175/JCLI-D-12-00584.1, 2013.

ESDD
5, 991–1012, 2014

Table 1. The differences of global annual [CO_2] concentration by 2005 and by 2100 between the emission- and concentration-driven (*E*-driven and *C*-driven) simulations (first two columns) with the ratios (in percentage) of the values in the second column over [CO_2] in 2100 in the concentration-driven simulations shown in parentheses (2nd column), the 20 yr average global surface air temperature differences between 2081–2100 and 1850–1869/1861–1880 in the *C*- and *E*-driven simulations (3rd and 4th columns) and their differences (between *E*- and *C*-driven simulations) with an asterisk indicating the statistical significance at $P < 0.01$ (5th column), and the correlation coefficients (all significant at $P < 0.01$) between simulated surface air temperature and the observation (from HadCRUT4.2; Morice et al., 2012) during the historical period (from 1850 or 1861 to 2005) (last two columns).

	Concentration difference [ppm]		Temperature difference [K]			Correlation	
	by 2005	by 2100	*C*-driven	*E*-driven	diff	*C*-driven	*E*-driven
BNU-ESM	+5.3	+62.1 (6.6)	5.30	5.58	+0.27*	0.858	0.842
CanESM2	+7.8	+111.2 (11.8)	5.33	5.74	+0.42*	0.771	0.765
CESM1-BGC	+18.3	+200.7 (21.4)	4.36	4.97	+0.61*	0.844	0.852
GFDL-ESM2G	+9.6	+50.6 (5.4)	3.23	3.29	+0.06	0.689	0.703
GFDL-ESM2M	+17.1	+48.6 (5.2)	3.12	3.23	+0.11	0.720	0.743
INMCM4	+1.3	−19.7 (−2.1)	3.11	2.99	−0.11*	0.849	0.833
MIROC-ESM	+9.9	+207.3 (22.1)	5.47	6.50	+1.03*	0.862	0.860
MIP-ESM-LR	−3.0	+26.2 (2.8)	4.26	4.29	+0.02	0.782	0.843
Multimodel Mean	+8.3	+85.9 (9.1)	4.27	4.57	+0.30*	0.800	0.805
Median	+8.7	+56.3 (6.0)	4.31	4.63	+0.19*	0.813	0.838

ESDD
5, 991–1012, 2014

Table 2. Temperature-concentration feedback coefficients α (K per 100 ppm) and α' (K; shown in parentheses) which are computed from Eqs. (1) and (2). All the values are significant at the 1 % level. The observed value is computed using the data from GLOBALVIEW-CO2 (2012) and HadCRUT4.2 (Morice et al., 2012).

	Concentration-driven		Emission-driven	
	1980–2005	2075–2100	1980–2005	2075–2100
BNU-ESM	1.87 (6.67)	0.55 (4.54)	1.85 (6.66)	0.50 (4.42)
CanESM2	2.04 (7.26)	0.62 (5.15)	1.88 (6.76)	0.59 (5.42)
CESM1-BGC	1.57 (5.60)	0.50 (4.09)	1.70 (6.30)	0.42 (4.14)
GFDL-ESM2G	2.07 (7.41)	0.46 (3.80)	1.03 (3.80)	0.38 (3.32)
GFDL-ESM2M	1.26 (4.50)	0.41 (3.34)	0.98 (3.65)	0.40 (3.47)
INMCM4	0.54 (1.94)	0.34 (2.80)	0.96 (3.44)	0.36 (2.93)
MIROC-ESM	1.27 (4.55)	0.74 (6.08)	1.40 (5.14)	0.73 (7.09)
MPI-ESM-LR	0.95 (3.38)	0.57 (4.76)	1.71 (6.14)	0.46 (3.86)
Multimodel mean	1.45 (5.16)	0.52 (4.32)	1.44 (5.24)	0.48 (4.33)
Multimodel median	1.42 (5.08)	0.52 (4.32)	1.55 (5.64)	0.44 (4.00)
Observation	1.23 (4.39)	–	1.23 (4.39)	–

ESDD
5, 991–1012, 2014

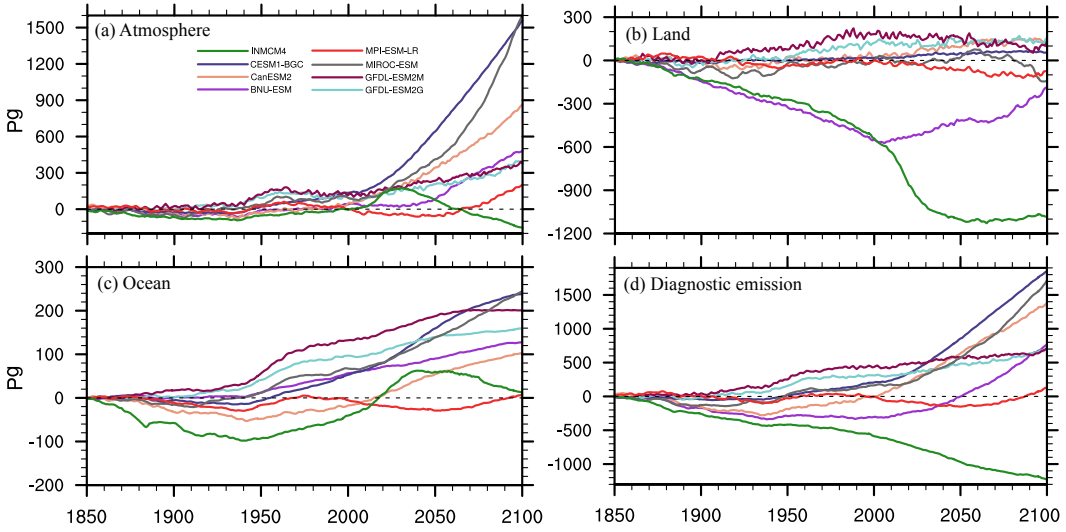

Figure 1. The annual differences between the emission- and concentration-driven simulations during 1850–2100: **(a)** atmospheric CO_2 mass, accumulated net carbon uptake by the land **(b)** and ocean **(c)**, and **(d)** diagnostic accumulated emissions computed as the sum of variations in the atmospheric, terrestrial and oceanic carbon pools. All ordinate units are converted to Pg CO_2, and positive values denote increment into the corresponding carbon pool.

ESDD
5, 991–1012, 2014

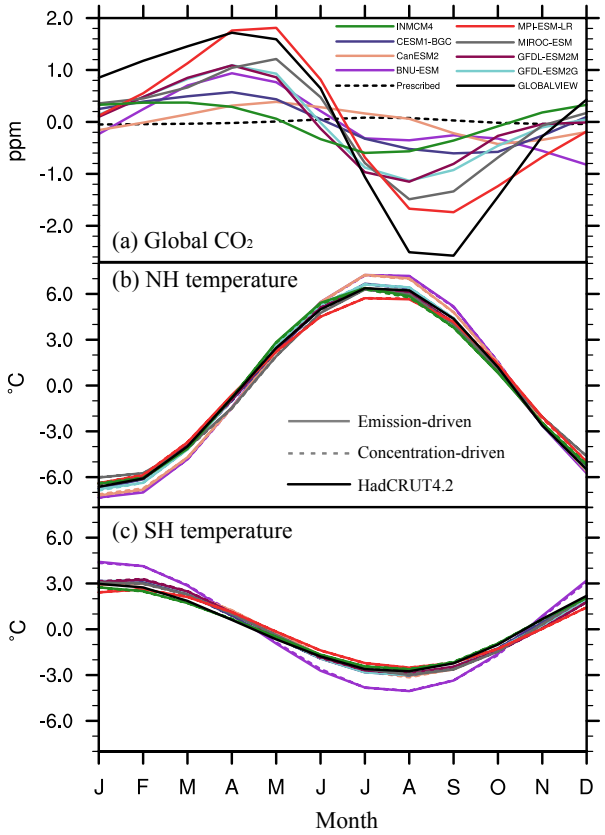

Figure 2. Seasonal cycles of [CO_2] (ppm) **(a)**, surface air temperature (°C) in the Northern Hemisphere **(b)** and in the Southern Hemisphere **(c)** during 1980–2011 after removing the annual mean and the trend. The observed values denoted by the solid black lines are from GLOBALVIEW-CO2 (2012) and HadCRUT4.2 (Morice et al., 2012) for the same period.

ESDD
5, 991–1012, 2014

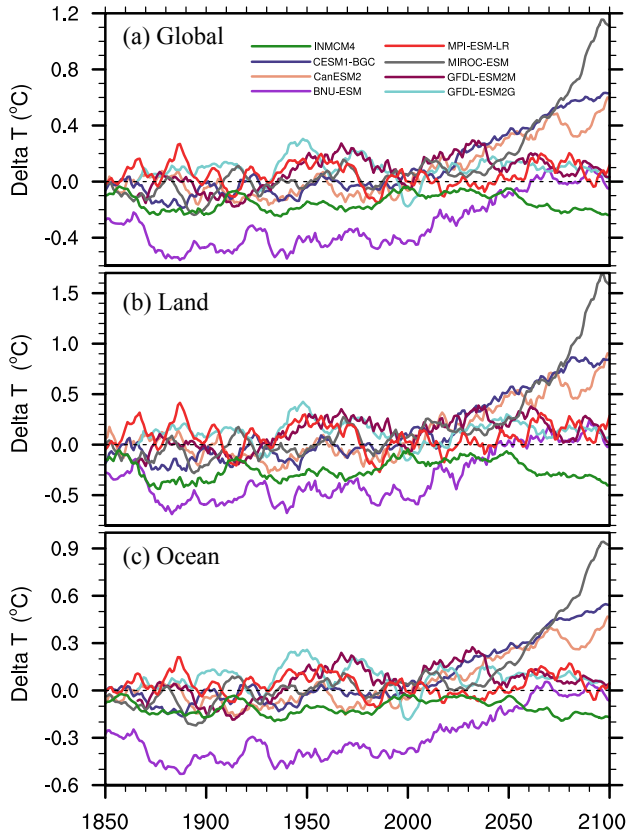

Figure 3. The 11 yr running mean of annual global **(a)**, terrestrial **(b)**, and oceanic **(c)** surface air temperature differences between the emission- and concentration-driven simulations.

ESDD
5, 991–1012, 2014

Differences in carbon cycle and temperature projections

P. Shao et al.